Molecular Dynamics Simulations of Lithium Alkyl Carbonates

Oleg Borodin,* Grant D. Smith, and Peng Fan

Department of Materials Science & Engineering, 122 South Central Campus Drive, Room 304, University of Utah, Salt Lake City, Utah 84112-0560

Received: June 22, 2006; In Final Form: August 11, 2006

A quantum chemistry-based many-body polarizable force field has been developed for two model solid-electrolyte interphase (SEI) components: dilithium ethylene dicarbonate (Li_2EDC) and lithium methyl carbonate (LiMC). Molecular dynamics (MD) simulations of amorphous Li_2EDC and LiMC were performed at temperatures from 393 to 600 K. Simulations reveal that Li^+ is coordinated by ∼4.6 oxygen atoms from $-COO^-$ groups coming from different alkyl carbonate molecules. Charge transport in Li_2EDC was found to be almost entirely due to Li^+. The temperature dependence of the ionic conductivity of the SEI model compounds Li_2EDC and LiMC was found to be significantly stronger than that of liquid electrolytes (e.g., ethylene carbonate + LiTFSI), yielding extrapolated conductivities of the Li_2EDC on order of 10^{-10} S/cm at −30 °C.

I. Introduction

Li-ion batteries are widely used in portable electronics and are primary candidates for use in hybrid electric vehicles. However, further progress in the understanding of current materials and the synthesis of novel electrode and electrolytes is needed to improve battery performance especially at low temperatures. Choice of the most suitable electrolyte is a complicated task as it should comply with a number of often conflicting requirements such as high conductivity and transference number, good mechanical properties, the ability to form good interfacial contact with electrodes, good electrochemical stability, ease of fabrication, low flammability, low toxicity, and low production cost.[1] High ionic conductivity of an electrolyte is necessary but not sufficient for Li^+ transport from anode to cathode and back. The ability of an electrolyte to form a stable and conductive passivation layer on both electrodes is also required for efficient battery operation especially at high discharge rates. Because passivation films act like electrolytes in their conductive properties they are called solid electrolyte interphases (SEIs). The chemical composition and morphology of the SEI on anode have been recently reviewed.[1,2] While the exact composition of the SEI is dependent on the electrolyte chemistry, salt, and electrode materials, the presence of crystalline LiO_2, Li_2CO_3 in the inner layer of the SEI in contract with the electrode, and amorphous lithium alkyl carbonates in the outer SEI layer in contact with the electrolyte has been observed for the majority of carbonate-based electrolytes in contact with the anode.[1,4−6] Similar species together with polyethercarbonates have been speculated to be present in the cathode passivation layer.[1]

An SEI layer resistance comparable to bulk electrolyte resistance has been observed at low temperatures indicating that the SEI transport properties could be as important as bulk electrolyte conductivities for efficient battery operation.[1] Most efforts to understand the SEI have focused on identification of SEI components and reduction mechanisms,[1] while little is known about electrochemical and transport properties of SEI components, especially those located next to electrolyte. Only recently, synthesis and characterization studies of lithium alkyl carbonates by nuclear magnetic resonance and Fourier transform infrared spectroscopy (FTIR), thermal analyses, and X-ray photoelectron spectroscopy have been reported.[7,8] However, we are not aware of reports on lithium transport properties of lithium alkyl carbonates. While quantum chemistry studies[9] of the gas-phase complexes of lithium alkyl carbonates have provided insight into lithium coordination by alkyl carbonates, extrapolating the gas-phase results into bulk properties of lithium alkyl carbonates is cumbersome and is often inconclusive.

Inspired by the ability of molecular dynamics (MD) simulations with many-body polarizable force fields to predict lithium transport in liquid electrolytes,[10,11] polymer electrolytes,[12] and ionic liquids,[13,14] we have investigated of two amorphous lithium alkyl mono- and dicarbonates: lithium methyl carbonate (LiMC) and dilithium ethylene carbonate (Li_2EDC), respectively, shown in Figure 1a,b. These compounds are common components of the outer part of SEI[1,3,7] and probably exist in a disordered state because of the high fraction of other components present inhibiting formation of the crystalline phase. In contrast to the previous subnanosecond long MD simulation study[15] of Li_2EDC performed at room temperature, where Li_2EDC melt was not simulated long enough to allow equilibration, we performed our simulations at high enough temperature (500−600 K) to ensure equilibration on the time scale accessible to simulations. We then gradually decrease the simulation temperature to obtain temperature dependence of structural and transport properties.

We begin this paper by outlining in Section II development of the quantum chemistry-based force field for lithium alkyl carbonate model compounds. In Section III the MD simulation methodology is presented, followed by simulation results and discussion of thermodynamic, structural, and transport properties of the LiMC and Li_2EDC SEI components in Sections IV and V.

II. Force Field Development

A. Force Field Form. Following our previous work[10−12,16,17] on lithium transport in carbonate liquid electrolytes, polymer

10.1021/jp0639142 CCC: $33.50
Published on Web 10/17/2006

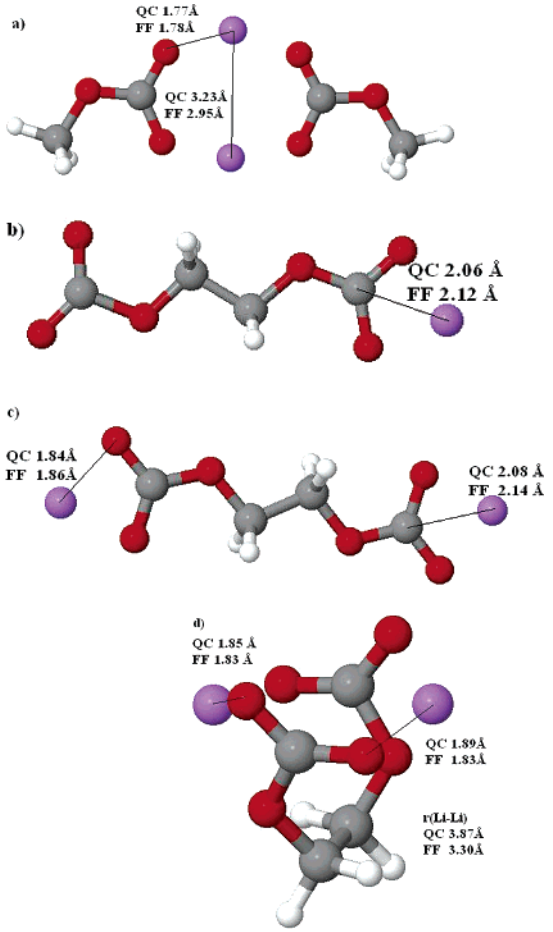

Figure 1. The B3LYP/aug-cc-pvDz optimized complex geometries of lithium alkyl carbonates. Selected distances from MM optimizations utilizing developed force field (FF) are also shown.

electrolytes, and ionic liquids, we utilized the potential energy function $U^{tot}(\mathbf{r})$ for the ensemble of atoms, represented by the coordinate vector $\mathbf{r}$,

$$U^{tot}(\mathbf{r}) = U^{NB}(\mathbf{r}) + \sum_{bends} U^{BEND}(\theta_{ijk}) + \sum_{torsions} U^{TORS}(\phi_{ijkl}) \quad (1)$$

The contributions due to bends $U^{BEND}(\theta_{ijk})$ and torsions $U^{TORS}(\phi_{ijkl})$ are given by

$$U^{BEND}(\theta_{ijk}) = \frac{1}{2}k^{BEND}_{\alpha\beta\gamma}(\theta_{ijk} - \theta_{ijk}{}^{0})^2 \quad (2)$$

$$U^{TORS}(\phi_{ijkl}) = \sum_{n}\frac{1}{2}k^{TORS}_{\alpha\beta\gamma\delta}[1 - \cos(n\phi_{ijkl})] \quad (3)$$

where θ_{ijk} and $\theta_{ijk}{}^{0}$ are the instantaneous and "natural" bending angle for atoms i, j, and k, and ϕ_{ijkl} is the dihedral angle for atoms i, j, k, and l. The $k^{BEND}_{\alpha\beta\gamma}$ and $k^{TORS}_{\alpha\beta\gamma\delta}$ are the bend force constant and torsional parameter, respectively. The α, β, γ, and δ denote atom type for atoms i, j, k, and l, respectively. Bond lengths were constrained in all simulations to allow use of a larger simulation time step. The nonbonded energy $U^{NB}(\mathbf{r})$ consists of the sum of the two-body repulsion and dispersion energy $U^{RD}(\mathbf{r})$, the energy due to interactions of fixed charges $U^{coul}(\mathbf{r})$ and the polarization energy $U^{pol}(\mathbf{r})$ arising from the interaction of induced dipoles with fixed charges and other

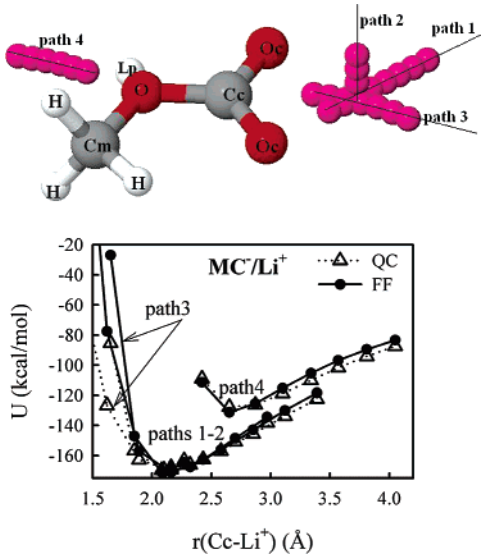

Figure 2. Nonbonded part of the binding energy of Li^+/MC^- from MP2/aug-cc-pvDz quantum chemistry calculations and force field. The B3LYP/aug-cc-pvDz geometry of the optimized Li^+/MC^- complex was used in all calculations. The Oc oxygen atoms are called carboxyl oxygen, while the oxygen in the C−O−C group is called ether oxygen EO.

induced dipoles,

$$U^{NB}(\mathbf{r}) = U^{RD}(\mathbf{r}) + U^{coul}(\mathbf{r}) + U^{pol}(\mathbf{r}) = \sum_{i>j}\left(A_{\alpha\beta}\exp(-B_{\alpha\beta}r_{ij}) - C_{\alpha\beta}r_{ij}{}^{6} + D\left(\frac{12}{B_{\alpha\beta}r_{ij}}\right)^{12}\right) + \sum_{i>j}\left(\frac{q_iq_j}{4\pi\epsilon_0 r_{ij}}\right) - 0.5\sum_i \vec{\mu}_i\vec{E}_i{}^{0} \quad (4)$$

Here the induced dipole at a force center i is $\vec{\mu}_i = \alpha_i\vec{E}_i^{tot}$, α_i is the isotropic atomic polarizability, $\vec{E}_i^{tot}$ is the total electrostatic field at the atomic site i due to permanent charges q_j and induced dipoles $\vec{\mu}_j$, ϵ_0 is the dielectric permittivity of vacuum, $\vec{E}_i^{0}$ is the electric field due to fixed charges only, $A_{\alpha\beta}$ and $B_{\alpha\beta}$ are the repulsion parameters, and $C_{\alpha\beta}$ is the dispersion parameter for interaction between atoms i and j that have atom types α,β. The magnitude of the term $D(12/B_{\alpha\beta}r_{ij})$,[12] $D = 0.0005$ kcal/mol is essentially zero at typical atom approaches, but becomes the dominant term at $r_{ij} < 1$ Å ensuring that $U^{RD}(\mathbf{r})$ is repulsive at unphysical close atom approaches. We also used the Thole screening that smears induced dipoles to prevent a polarization catastrophe from occurring as previously described.[10] The interaction between an induced dipole and a partial charge separated by 3 bonds was scaled by 0.8, providing an improved description of the electrostatic potential around molecules. In accord with our previous work,[10] we found that addition of an off-atom site is needed to improve the electrostatic potential description near electron lone-pairs situated at ether oxygen (EO) atoms. Instead of introducing two additional force centers to model the lone-pair contribution to the electrostatic potential around EO atoms, we used a single "extended charge" denoted as Lp that was situated at 0.5 Å from the oxygen atom along the C−O−C bisector as shown by Figure 2.

B. Quantum Chemistry Calculations and Force Field Fitting. As in previous quantum chemistry studies of Li^+ complexation to carbonates,[11] ethers,[11,18] and lithium halides,[18] a Li^+ basis set of the [8s4p3d/5s3p2d] type with an improved description of 1s orbitals is used. The aug-cc-pvDz basis is used

for carbonates as in our previous studies[11] of Li^+/carbonate complexes. The Gaussian 98 package[19] was used for all quantum chemistry calculations. The basis set superposition error (BSSE) correction has not been performed because our previous study[11] of Li^+/carbonate complexes carbonates utilizing the same basis sets showed that BSSE is less than 1 kcal/mol for a single ethylene carbonate(EC) complexing Li^+ and less than 2 kcal/mol for two EC molecules complexing Li^+.

We closely followed a previously described force field development methodology[10,11] that will be briefly described here. First, the atomic polarizabilities for atoms in the CH_3- and $-CH_2-CH_2-$ groups were assumed to be transferable from our previously developed transferable force field based on carbonates, alkanes, and ethers.[10] Second, atomic polarizabilities of atoms in the carbonate group were adjusted to match the polarization energy ($U^{pol}(\mathbf{r})$ in eq 4) of the MC^- anion in the presence of a test charge (e^+) calculated at the MP2/aug-cc-pvDz level at B3LYP/aug-cc-pvDz geometries along paths probing regions around MC^- as shown in Figure 2. The polarization energy $U^{pol}(\mathbf{r})$ at each location of the test charge (e^+) was calculated as the energy of the $MC^-/(e^+)$ complex minus the value of the electrostatic potential at the same point. Third, the electrostatic potential on a grid of evenly spaced points ($\sim 90^3$ points) around MC^-, EDC^{2-}, LiMC, and Li_2EDC, and the dipole $\vec{\mu}_i$ and quadrupole moment Θ_i of these molecules were calculated at the MP2/aug-cc-pvDz level. Partial charges were determined by minimizing $\chi^2(\vec{q})$

$$\chi^2(\vec{q}) = \sum_{i=1}^{M} \omega_i \left[\sum_{j=1}^{N_{GRID}} \frac{\omega^{\phi}}{N_{GRID}} (\phi_{ij}^{QC} - \phi_{ij}^{FF}(\vec{q}))^2 + \omega^{\vec{\mu}} (\vec{\mu}_i^{QC} - \vec{\mu}_i^{FF}(\vec{q}))^2 + \omega^{\Theta} (\Theta_i^{QC} - \Theta_i^{FF}(\vec{q}))^2 \right] \quad (5)$$

where $\vec{q}$ represents the partial atomic charges, ϕ_{ij}^{QC} and ϕ_{ij}^{FF} are the electrostatic potential for the *i*th molecule (or complex) at the *j*th grid point from quantum chemistry (QC) and molecular mechanics with use of developed force field (FF), $\vec{\mu}_i^{QC}$ and $\vec{\mu}_i^{FF}$ are dipole moments, and Θ_i^{QC} and Θ_i^{FF} are quadrupole moments for a molecule *i* from QC and FF, respectively. The weights ω_i (0.5 for MC^-, 1 for EDC^{2-}, 0.2 for LiMC, and 0.4 for Li_2EDC) are given for each molecule. The relative weights for fitting electrostatic potential, dipole, and quadrupole moments ω^{φ}, $\omega^{\vec{\mu}}$, and ω^{Θ} were set to 1.0, 0.2, and 0.1, respectively. The electrostatic potential points closer than 1.8 Å to oxygen, 1.5 Å to hydrogen, and 2.5 Å to carbon atoms were excluded from fitting together with points that are further than 4 Å as discussed elsewhere.[20] Fourth, atomic polarizability of the carboxyl oxygen and carbon (labeled Oc and Cc in Figure 2) was slightly adjusted to obtain the best fit to the nonbonded binding energy $U^{NB}(\mathbf{r})$ of the Li^+/MC^- complex calculated at the MP2/aug-cc-pvDz level at B3LYP/aug-cc-pvDz geometries resulting in the fit shown in Figure 2. Final atomic polarizabilities and charges are given in Table 1. The traces of the molecular polarizability tensor calculated from atomic polarizabilities (α_i) from FF and QC at the B3LYP/aug-cc-pvDz level are 5.6 and 7.4 $Å^3$ for MC^- anion, and 11 and 13.7 $Å^3$ for EDC^{2-} anion, respectively. The polarizability of the anions from FF is 20−25% lower than that from QC. However, anion polarizability is expected to be significantly reduced in a condensed phase[21] from the gas-phase values, suggesting that force field polarizabilities might be in line with condensed-phase values.

Finally, bend force constants and out-of-plane deformations were transferred from the previous force field.[10] The equilibrium bend angles were fit to geometries obtained at the B3LYP/aug-cc-pvDz level for EDC^{2-} and MC^-, while bond lengths were set to the average bond length values for these compounds found at the same level. Torsional parameters (eq 3) were fit to conformational energetics of EDC^{2-} as shown in Table 2. All other force field parameters are listed in the Supporting Information section.

TABLE 1: Atomic Charge and Polarizability Used in Developed Force Field

atom type[a]	charge (e)	polarizability ($Å^3$)
Oc	−0.7658	0.65
O	−0.0217	1.05
Cc	0.6556	0.9
C (ethylene unit in EDC^{2-})	−0.1097	0.50
Cm	−0.2197	0.05
Lp	−0.2126	0
H	0.1100	0.46
Li	1.0	0.0

[a] Atom types are shown in Figure 2.

TABLE 2: Conformational Energies (in kcal/mol) of EDC^{2-} from Quantum Chemistry Calculations Using Aug-cc-pvDz Basis Set at B3LYP/Aug-cc-pvDz Geometries and from Force Field[a]

conformer $C_c-O-C-C-O-C_c$	HF	B3LYP	MP2	FF
level of theory for single-point energy calculations				
ttt	0	0	0	0
tgt	3.2	4.3	3.5	3.5
barriers and geometries with a constrained angle				
tgt ↔ ttt	3.8	5.2	4.3	4.3
tct	14.1	15.9	14.6	14.2
120*tt	1.4	2.3	1.8	2.0
105*tt	1.8	2.7	2.0	2.4
75*tt	3.5	4.1	3.2	3.3
60*tt	5.3	6.5	4.7	4.8
ctt	12.2	13.3	12.2	13.6
ctg^-	12.0	13.7	12.0	11.4

[a] t = trans, g = gauche, (g^- = gauche minus), c = cis. The asterisk denotes constrained torsional angle.

TABLE 3: Binding Energy (in kcal/mol) for Lithium Alkyl Carbonate[a] Complexes from Quantum Chemistry Calculations[b] Using Aug-cc-pvDz Basis Set for Anions and [8s4p3d/5s3p2d] Basis Set for Li along with Results of MM Minimization Utilizing Developed FF

	HF[a]	B3LYP[a]	MP2 (frozen core)[a]	MM using FF
$(LiMC)_2$	−391.3	−382.7	−373.5	−382.2
EDC_{ttt}^{2-}/Li^+	−215.8	−215.1	−210.6	−212.3
$EDC_{ttt}^{2-}/2Li^+$	−385.2	−381.7	−373.2	−381.1
$EDC_{g^-g^+g^-}^{2-}/2Li^+$	−405.6	−406.3	−402.4	−414.8
$(EDC_{g^-g^+g^-}^{2-}/2Li^+) - (EDC_{ttt}^{2-}/2Li^+)$	−20.5	−24.6	−29.1	−33.7

[a] EDC_{ttt}^{2-} and $EDC_{g^-g^+g^-}^{2-}$ denote the ttt and $g^-g^+g^-$ conformers of ethylene dicarbonate. [b] Geometry optimization was performed at the B3LYP/(aug-cc-pvDz for anion and [8s4p3d/5s3p2d] for Li) level.

Next, we perform force field validation by evaluating the accuracy of its predictions of binding energies and structural parameters for the complexes of one and two lithiums with EDC^{2-} or an MC^-_2 dimer shown in Figure 1. Table 3 summarizes results of molecular mechanics (MM) optimizations utilizing the developed force field and QC results. In accord with previous studies[11] of Li^+ binding to EC and dimethyl ketone, we observe a tendency for the magnitude of the binding energy to be HF > B3LYP > MP2. The MM predictions lie between B3LYP and MP2 QC results for all complexes with the exception of the $EDC^{2-}/2Li^+$ complex in $g^-g^+g^-$ conforma-

TABLE 4: MD Simulation Length and Alkyl Carbonate Densities

T (K)	run length (ns)	density (kg m^{-3})
	Li_2EDC	
600	2.4	1568
500	9	1598
423	8	1633
393	9	1643
	LiMC	
500	1	1300
423	12	1337
393	9	1359

tion, where MM predicts a binding energy ~9 kcal/mol (or 2.2%) stronger than the QC results. Nevertheless, we think that force field performance is adequate taking into account the uncertainty of quantum chemistry values. Note that the distances between Li^+ and carbon (Cc) and oxygen (Oc) atoms from QC are in good agreement with those predicted by MM calculations as shown in Figure 1. However, a typical Li^+-Oc distance in a Li_2EDC complex of ~1.85 Å is longer than the 1.65 Å distance predicted by the COMPASS force field and previously reported[15] from MM optimization of the Li_2EDC complex. The shorter separation by the COMPASS force field indicates that the COMPASS force field predicts more compact lithium alkyl carbonate structures than QC and our current force field. This will result in a higher density of lithium alkyl carbonates from the COMPASS force field compared to predictions from MD simulations with the current force field as discussed below.

III. Molecular Dynamics Simulation Methodology

A polarizable version of the MD simulations code Lucretius[22] was used for all MD simulations. The Li_2EDC and LiMC electrolytes consisted of 400 lithium cations and a corresponding number of alkyl carbonate anions. The systems were created in the gas phase with the initial periodic cell (box) size of ~100 Å. The cell was shrunk in MD simulations by using a Brownian dynamics algorithm[23] over a period of 0.3 ns at 600 K, with subsequent equilibration in the NPT ensemble for 0.8 ns at 600 K for Li_2EDC and 500 K for LiMC. Then Li_2EDC and LiMC were simulated in a series of NPT and NVT runs at each temperature reported in Table 4. Initial configuration at each temperature was taken from the final configuration of the next higher temperature. NPT runs of typically 0.5−1 ns were used to obtain equilibrium box size at 1 atm of pressure. This box size was used in the subsequent NVT runs.

A Nose−Hoover thermostat and a barostat[22] were used to control the temperature and pressure with characteristic frequencies of 10^{-2} and 10^{-3} fs^{-1}, respectively. Bond lengths were constrained by using the Shake algorithm[23] to utilize a larger time step. The Ewald summation method was used for treatment of long-range electrostatic forces between partial charges and between partial charges and induced dipoles. A tapering function was used to drive the induced dipole−induced dipole interactions to zero at a cutoff of 10 Å, with scaling starting at 9 Å. A multiple time step reversible reference system propagator algorithm was employed,[24] with a time step of 0.5 fs for bonding, bending, and torsional motions, a 1.5 fs time step for nonbonded interactions within a 6.5 Å sphere, and a 3.0 fs time step for nonbonded interactions between 6.5 and 10.0 Å and the reciprocal space part of the Ewald summation.[23] The Ewald convergence parameter α was set to 8 Å. The number of reciprocal space vectors was set to 6^3.

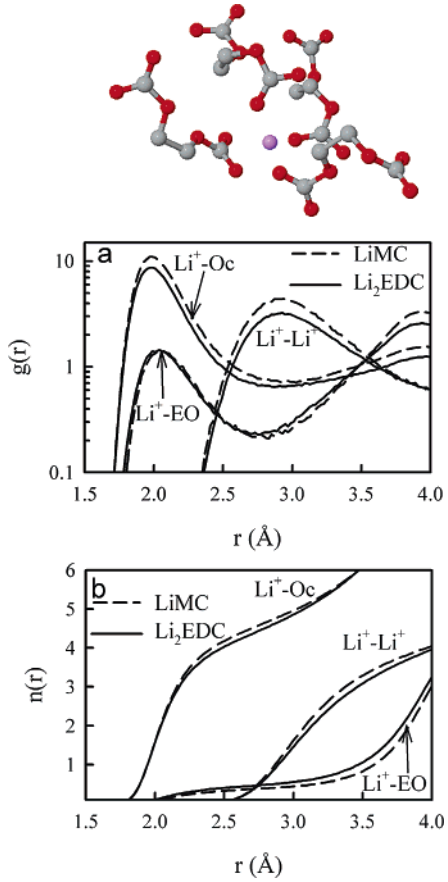

Figure 3. Radial distribution function ($g(r)$) and running coordination number ($n(r)$) for alkyl carbonates at 393 K. A representative snapshot of the Li^+ coordination by EDC^{2-} is also shown.

IV. Thermodynamic and Structural Properties

A. Density. The density of the simulated alkyl carbonates from MD simulations is given in Table 4. Extrapolation of the Li_2EDC density to room temperature yields a value of ~1690 kg/m^3 that is noticeably lower than the previously predicted density of Li_2EDC of 1860 kg/m^3 with use of the COMPASS force field.[15] This difference is, at least partially, attributed to the shorter Li−Oc separation in lithium alkyl carbonate predicted by the COMPASS force field for gas-phase clusters compared to developed force field predictions.

B. Structure. We begin the exploration of Li_2EDC and LiMC structure by examining the Li^+-Oc, Li^+-EO, and Li^+-Li^+ radial distribution functions (RDF) as shown in Figure 3a. Li^+ is strongly coordinated by carboxyl oxygen atoms with the most probable separation distance of 1.98 Å for both the mono- and dicarbonate. Analysis of RDFs indicates that the probability of a Li^+ being coordinated by EO is almost an order of magnitude lower than being coordinated by Oc, while positions of the first peak are similar for the Li^+-Oc and Li^+-EO RDFs. The running Li^+ coordination numbers $n(r)$ for the Li^+-X pair depict the number of atoms for species X within a distance r. The $n(r)$ for Li^+-X (X = Oc, EO, Li^+) are shown in Figure 3b. Within the first Li^+-Oc coordination shell of 2.8 Å, corresponding to the first minima of the Li^+-Oc RDF, we observe 4.5 and 4.7 carboxyl oxygen atoms coordinating a Li^+ for Li_2EDC and LiMC, respectively. The majority of Li^+ (82−87%) have carbonate molecules contributing only one oxygen atom to the Li^+ first coordination shell for Li_2EDC and LiMC at 423 K, thus Li^+ cations primarily bridge different carbonate molecules (see the snapshot in Figure 3). Further analysis

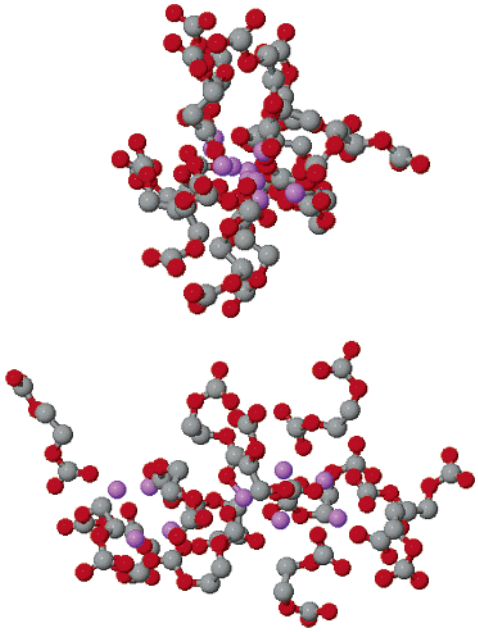

Figure 4. A part of the Li_2EDC simulation cell demonstrating multiple lithiums being coordinated by EDC^{2-} anions. Li^+ cations are shown in purple.

indicates that less than 11% of Li^+ form complexes shown in Figure 1d, where the Li^+ cations are bridging carbonate groups from both ends of the EDC^{2-} anion. This is consistent with the population of the $g^+g^-g^+$ conformer of EDC^{2-} that allows intermolecular bridging of carbonate groups (see Figure 1d) being less than 12% in the Li_2EDC simulations. Thus, the intermolecular bridging via Li^+ dominates over intermolecular bridging. The Li^+ coordination environment in alkyl carbonates has similarities with the Li^+ coordination by sulfonyl groups of bis(trifluoromethanesulfonyl)imide ($TFSI^-$) in *N*-methyl-*N*-propylpyrrolidinium$^+TFSI^-$ ionic liquid doped with LiTFSI,[14] where a Li^+ is coordinated by approximately four oxygen atoms also coming primarily from different anions.

Figure 3 also shows significant Li^+-Li^+ correlations with the most probable distance of 3 Å. Each Li^+ has approximately 4 other Li^+ within its first coordination shell of 4 Å. Figure 4 shows a typical coordination of lithium cations, in which pathways for the Li^+ conduction by exchanging carbonate groups are formed. Such pathways percolate through the simulation cell as shown in Figure 5, where nearest Li^+ cations are connected. The validity of this picture for Li^+ conduction will be discussed below.

V. Transport and Dynamic Properties

A. Ion Self-Difffusion. The self-diffusion coefficient D_i for species i was calculated by using the Einstein relation[23]

$$D_i = \lim_{t\to\infty} \frac{\langle \mathrm{MSD}_i(t) \rangle}{6t} \tag{6}$$

where $\mathrm{MSD}_i(t)$ is the mean-square displacement of the molecule center of mass for species i (cation or anion) during time t and $\langle\,\rangle$ denotes an ensemble average. In our simulations Li^+ cations reached the diffusive regime only for simulations at temperatures of 500 K and higher for Li_2EDC and 423 K and higher for LiMC. The Li^+ motion is subdiffusive (slope is less than one on the log−log plot) for the other temperatures. It is necessary to reach the diffusive regime to accurately extract a self-diffusion coefficient from MD simulations. As the temperature decreases,

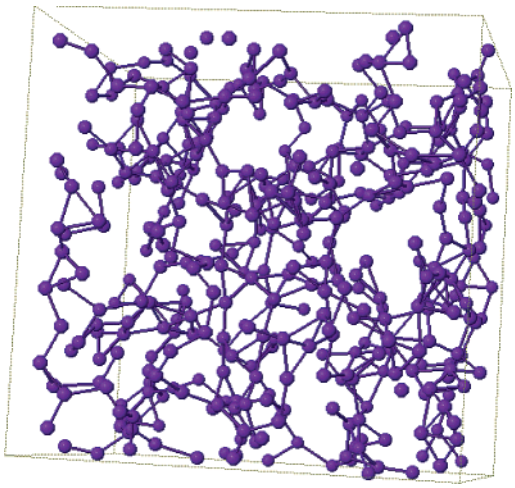

Figure 5. A simulation cell of Li_2EDC showing only Li^+ with the nearest neighbors connected.

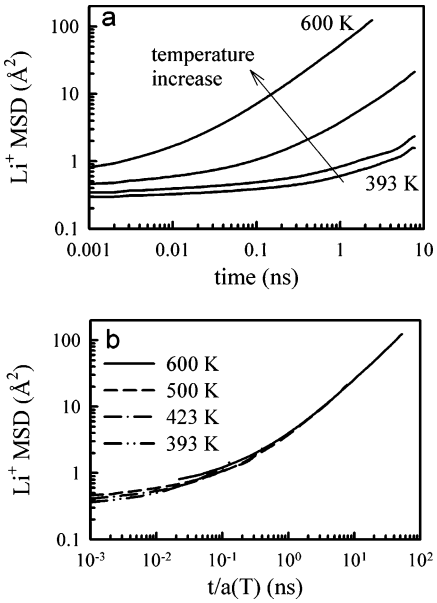

Figure 6. Li^+ mean-square displacements for Li_2EDC.

longer simulations are required to reach the diffusive regime, as long as 100 ns for Li_2EDC at 393 K. Such simulations are very expensive, however, especially using the many-body polarizable potentials we employed, thus posing significant difficulties for obtaining the Li^+ self-diffusion coefficient at low temperatures. To estimate the ion self-diffusion coefficient as accurately as possible at low temperatures, we assumed that the $\mathrm{MSD}_i(t)$ values at different temperatures can be superimposed onto each other by scaling the time axis as shown in Figure 6. As all curves superimpose on each other well for the Li^+ displacements larger than 1 Å^2, we conclude that it is a reasonable assumption. Similar behavior was seen in previous simulations[12] of PEO/LiTFSI. The self-diffusion coefficients of all ions are determined as

$$D_i(T) = D_i(500\mathrm{K})/a_i(T) \tag{7}$$

where $D_i(500\mathrm{K})$ was obtained utilizing eq 6 at 500 K and $a_i(T)$ is the temperature-dependent time-shift factor obtained by superimposing the $\mathrm{MSD}_i(t)$ as shown in Figure 6b for the Li^+ cation in Li_2EDC.

The ion diffusion coefficients are shown in Figure 7. The EDC^{2-} diffusion coefficient is more than an order of magnitude

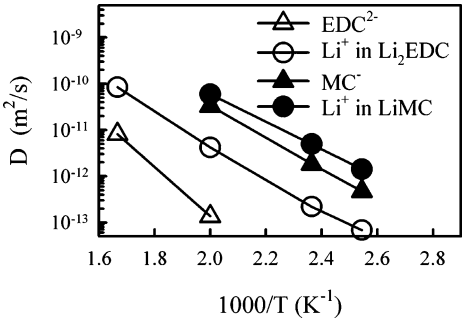

Figure 7. Ion self-diffusion coefficients from MD simulations.

lower than that for the Li^+ cation indicating that Li^+ is responsible for most of the charge transport in Li_2EDC. In contrast, the MC^- anion diffusion coefficient is only a factor of 2−3 smaller than that of Li^+ with the difference becoming larger as temperature decreases. Finally, Li^+ transport is approximately an order of magnitude faster in LiMC than in Li_2EDC. This is probably due to the significantly faster exchange of carbonate groups by Li^+ enhanced by faster local dynamics of the MC^- anion compared to EDC^{2-} and a small contribution from the Li^+ moving together with MC^- as revealed by analysis of the correlations between cation−anion motion reported in the next section.

B. Conductivity. Ionic conductivity can be extracted from the MD simulations by using the Einstein relation[23]

$$\lambda = \lim_{t\to\infty} \lambda^{app}(t) = \lim_{t\to\infty} \frac{e^2}{6tVk_BT} \sum_{i,j}^{N} z_i z_j \langle ([\mathbf{R}_i(t) - \mathbf{R}_i(0)])([\mathbf{R}_j(t) - \mathbf{R}_j(0)]) \rangle \quad (8)$$

where e is the electron charge, V is the volume of the simulation box, k_B is Boltzmann's constant, T is the temperature, t is time, z_i and z_j are the charges of ions i and j in electrons, and $\mathbf{R}_i(t)$ is the displacement of the ion i during time t. The summation is performed over all ions, while $\langle\ \rangle$ denote the average over all time origins used in the calculation, and N is the total number of ions in the simulation box. $\lambda^{app}(t)$ is the apparent time-dependent conductivity whose long-time limit is the zero-frequency ionic conductivity.

In a limit of completely dissociated and uncorrelated ion motion, electrolyte conductivity is given by the long-time limit of $\lambda^{app}_{uncorr}(t)$,

$$\lambda^{app}_{uncorr}(t) = \frac{e^2}{Vk_BT}(z_+^2 n_+ D_+^{app}(t) + z_-^2 n_- D_-^{app}(t)) = \frac{e^2}{6tVk_BT} \sum_{i}^{N} z_i^2 \langle [\mathbf{R}_i(t) - \mathbf{R}_i(0)]^2 \rangle \quad (9)$$

where n is the number of positive and negative charge carriers denoted by subscripts "+" and "−" and $D^{app}(t)$ is the apparent self-diffusion coefficient that is equal to $MSD_i(t)/6t$, where t is time. Conductivity λ is connected to $\lambda_{uncor.}$ via the degree of uncorrelated ion motion (α) given by

$$\alpha = \frac{\lambda}{\lambda_{uncorr}} = \lim_{t\to\infty} \alpha(t) = \lim_{t\to\infty} \frac{\lambda^{app}(t)}{\lambda^{app}_{uncorr}(t)} \quad (10)$$

Thus, $\alpha = 1$ corresponds to uncorrelated ion motion, while $\alpha = 0$ if all of the cations only move together with anions. The degree of uncorrelated motion (α) was extracted from the subdiffusive regime, where adequate statistics are present in order to accurately estimate α as described in our previous studies of ionic liquids.[13,14] We found α to be around 0.5($\pm$0.2) for LiMC from eq 10 indicative that approximately half of the charge transport in LiMC is correlated. In EDC^{2-} melt α is between 0.8 and 1 with error bars $\pm$0.2 indicating that ion motion is largely uncorrelated. This is consistent with a much faster Li^+ transport past EDC^{2-} anions as seen from ion self-diffusion analysis shown in Figure 7, especially at lower temperatures. Thus Li_2EDC shows single-ion conductor-like behavior and its conductivity is calculated with eq 9, where the first term $z_+^2 n_+ D_+^{app}(t)$ reflects Li^+ transport and dominates over the second term $z_-^2 n_- D_-^{app}(t)$ that reflects anion transport.

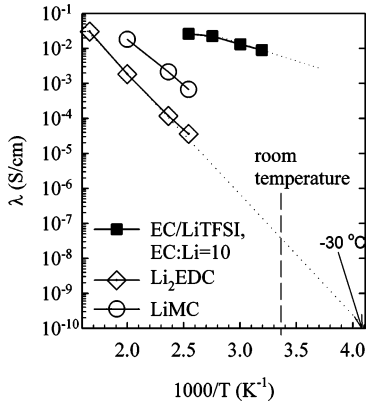

Figure 8. Alkyl carbonate and EC/LiTFSI[16] conductivity from MD simulations.

The ionic conductivities for the lithium alkyl carbonates were calculated from ion self-diffusion coefficients and α with eqs 9 and 10 and are given in Figure 8. The high-temperature conductivity of alkyl carbonates is comparable to that of liquid electrolytes such as EC/LiTFSI.[16] However, the much stronger temperature dependence of alkyl carbonate conductivity compared to typical liquid electrolytes (e.g., EC/LiTFSI) leads to significantly lower conductivity of alkyl carbonates at lower temperature compared to liquid electrolytes. The extrapolated conductivity of Li_2EDC at −30 °C is on the order of 10^{-10} S/cm suggesting that an SEI comprised primarily of Li_2EDC with typical width[1] of ~10 nm would give rise to significant SEI layer resistance. Conductivity of LiMC is somewhat greater than that for Li_2EDC.

C. Li^+−Solvent Residence Time. The residence time autocorrelation function (ACF) $P(t)$ for the Li^+−Oc coordination to exist was calculated as follows,

$$P(t) = \frac{\langle H_{ij}(t) H_{ij}(0) \rangle}{\langle H_{ij}(0) H_{ij}(0) \rangle} \quad (11)$$

where $H_{ij}(t)$ is 1 if the ith Li^+ is coordinated by the jth carbonate oxygen, i.e., $r_{Li^+-Oc} < 2.8$ Å, and $\langle\ \rangle$ denotes average over all time origins and pairs. The residence time τ_{Li^+-Oc} was calculated as the integral from zero to infinity to the stretched exponential $\exp[-(t/\tau)^\beta]$ fits to the $P(t)$ ACF and is shown in Figure 9. The τ_{Li^+-Oc} gives a characteristic time scale for a Li^+ to exchange Oc solvating groups, which increases from subnanoseconds at 600 K for Li_2EDC and 500 K for LiMC to estimated values of hundreds of nanoseconds for Li_2EDC at 423 K and tens of nanoseconds for LiMC at 393 K. Temperature dependence of τ_{Li^+-Oc} is similar to that for the inverse diffusion coefficients that characterize the time scale of translational motion indicating coupling of solvent exchange with lithium translational motion.

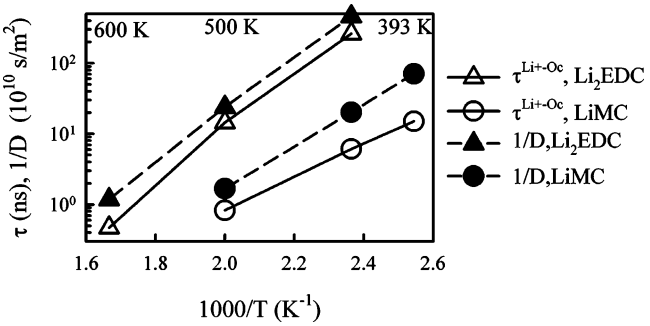

Figure 9. The Li^+-Oc residence time (τ^{Li+-Oc}) and inverse diffusion coefficients for alkyl carbonates.

We would like to answer if it is possible for a Li^+ to move past carbonate solvating groups that form its first complexation shell or cage without breaking the cage apart. To answer this question we compare the Li^+ residence time next to the carbonate group with the residence time for a carbonate group to have another carbonate group nearby. If a Li^+ cation resides much less time near a carbonate compared to the time the carbonate groups stay together with each other and form a cage, the Li^+ will move past (through) the cage formed by carbonate groups without its relaxation. We calculated the Li^+-Cc and $Cc-Cc$ residence times using 3.8 and 6.0 Å shell radii, respectively, by integrating $P(t)$ using eq 11. These residence times characterize Li^+ motion past carbonate groups and the lifetime of the cage of carbonate groups that is formed via bonding to Li^+ cations, respectively. We have found that the Li^+-Cc residence time is 6.5 times shorter than the $Cc-Cc$ residence times for Li_2EDC and 2.3 times shorter than those for LiMC. Thus, in the Li_2EDC melt Li^+ cations exchange numerous carbonate solvating groups before the cage created by EDC^{2-} molecules is relaxed, while in LiMC the time scale for Li^+ exchange of carbonate groups is comparable (2.3) to the relaxation time of the cage consisting of carbonate groups.

VI. Conclusions

A quantum chemistry-based many-body polarizable force field has been developed for lithium alkyl mono- and dicarbonates that adequately represents binding energetics of one and two lithiums to alkyl carbonates and conformational energetics of EDC^{2-}. This force field was utilized in MD simulations aimed at understanding structure and ion transport in amorphous alkyl carbonates at temperatures 393−600 K. We found that each Li^+ is coordinated by 4.5−4.7 carboxyl oxygens of EDC^{2-} or MC, with most carbonate groups contributing only one oxygen to the Li^+ first solvation shell. The lifetime of the cages formed by carbonate groups around a Li^+ cation in LiMC was comparable to the residence time of a Li^+ complexation of carbonate groups, while in Li_2EDC these cages lived longer than the residence time of a Li^+ near carbonate groups. This suggests the picture of lithium cations moving along conducting pathways in Li_2EDC is a reasonable first approximation.

Conductivity of Li_2EDC extrapolated to −30 °C was on the order of 10^{-10} S/cm indicating a significant resistance of this SEI layer component at low temperatures. The Li^+ motion accounted for most of the charge transport in Li_2EDC suggesting that Li_2EDC exhibits a single-ion conductor-like behavior. Conductivity of LiMC was up to an order of magnitude higher that that for Li_2EDC.

Acknowledgment. The authors are grateful for financial support of this work by the Assistant Secretary for Energy Efficiency and Renewable Energy, Office of FreedomCAR and Vehicle Technologies of the U.S. Department of Energy under Contract No. DE-AC02-05CH11231 on PO No. 6515401 (University of Utah). Stimulating discussions with Phil Ross (LBNL) are also acknowledged.

Supporting Information Available: Force field parameters used in simulation of alkyl carbonates. This material is available free of charge via the Internet at http://pubs.acs.org.

References and Notes

(1) Xu, K. *Chem. Rev.* **2004**, *104*, 4303.
(2) Peled, E.; Golodnitsky, D.; Menachem, C.; Bar-Tow, D. *J. Electrochem. Soc.* **1998**, *145*, 3482.
(3) Zhuang, G. V.; Xu, K.; Yang, H.; Jow, T. R.; Ross, P. N. *J. Phys. Chem. B* **2005**, *109*, 17567.
(4) Augustsson, A.; Herstedt, M.; Guo, J. H.; Edstrom, K.; Zhuang, G. V.; Ross, P. N.; Rubensson, J. E.; Nordgren, J. *Phys. Chem. Chem. Phys.* **2004**, *6*, 4185.
(5) Zhuang, G. V.; Xu, K.; Jow, T. R.; Ross, P. N. *Electrochem. Solid State Lett.* **2004**, *7*, A224.
(6) Zhuang, G. V.; Yang, H.; Ross, P. N.; Xu, K.; Jow, T. R. *Electrochem. Solid State Lett.* **2006**, *9*, A64.
(7) Xu, K.; Zhuang, G. V.; Allen, J. L.; Lee, U.; Zhang, S. S.; Ross, P. N.; Jow, T. R. *J. Phys. Chem. B* **2006**, *110*, 7708.
(8) Dedryvere, R.; Leroy, S.; Martinez, H.; Blanchard, F.; Lemordant, D.; Gonbeau, D. *J. Phys. Chem. B* **2006**, *110*, 12986.
(9) Wang, Y. X.; Balbuena, P. B. *J. Phys. Chem. A* **2002**, *106*, 9582.
(10) Borodin, O.; Smith, G. D. *J. Phys. Chem. B* **2006**, *110*, 6279.
(11) Borodin, O.; Smith, G. D. *J. Phys. Chem. B* **2006**, *110*, 6293.
(12) Borodin, O.; Smith, G. D. *Macromolecules* **2006**, *39*, 1620.
(13) Borodin, O.; Smith, G. D. *J. Phys. Chem. B* **2006**, *110*, 11481.
(14) Borodin, O.; Smith, G. D.; Henderson, W. *J. Phys. Chem. B* **2006**, *110*, 16879.
(15) Tasaki, K. *J. Phys. Chem. B* **2005**, *109*, 2920.
(16) Borodin, O.; Smith, G. D. *J. Phys. Chem. B* **2006**, *110*, 4971.
(17) Borodin, O.; Smith, G. D.; Douglas, R. *J. Phys. Chem. B* **2003**, *107*, 6824.
(18) Smith, G. D.; Jaffe, R. L.; Partridge, H. *J. Phys. Chem. A* **1997**, *101*, 1705.
(19) Frisch, M. J.; et al. *GAUSSIAN 98*, Revision A.7; Gaussian, Inc.: Pittsburgh, PA 1998.
(20) Smith, G. D.; Borodin, O. Quantum Chemistry-Based Force Fields for Polymers. In *Molecular Simulation Methods for Predicting Polymer Properties*; Galiatsatos, V., Ed.; Wiley-Interscience: Hoboken, NJ, 2005; p 45.
(21) Morita, A.; Kato, S. *J. Chem. Phys.* **1999**, *110*, 11987.
(22) Smith, G. D.; Bedrov, D.; Byutner, O.; Borodin, O.; Ayyagari, C.; Sewell, T. D. *J. Phys. Chem. A* **2003**, *107*, 7552.
(23) Frenkel, D.; Smit, B. *Understanding Molecular Simulation*: *From Algorithms to Applications*, 2nd ed.; Academic Press: New York, 2002.
(24) Martyna, G. J.; Tuckerman, M.; Tobias, D. J.; Klein, M. L. *Mol. Phys.* **1996**, *87*, 1117.